nature photonics

ARTICLES

https://doi.org/10.1038/s41566-018-0136-1

Fibre multi-wave mixing combs reveal the broken symmetry of Fermi–Pasta–Ulam recurrence

Arnaud Mussot[1*], Corentin Naveau[1], Matteo Conforti[1], Alexandre Kudlinski[1], Francois Copie[1], Pascal Szriftgiser[1] and Stefano Trillo[2*]

In optical fibres, weak modulations can grow at the expense of a strong pump to form a triangular comb of sideband pairs, until the process is reversed. Repeated cycles of such conversion and back-conversion constitute a manifestation of the universal nonlinear phenomenon known as Fermi–Pasta–Ulam recurrence. However, it remains a major challenge to observe the coexistence of different types of recurrences owing to the spontaneous symmetry-breaking nature of such a phenomenon. Here, we implement a novel non-destructive technique that allows the evolution in amplitude and phase of frequency modes to be reconstructed via post-processing of the fibre backscattered light. We clearly observe how control of the input modulation seed results in different recursive behaviours emerging from the phase-space structure dictated by the spontaneously broken symmetry. The proposed technique is an important tool to characterize other mixing processes and new regimes of rogue-wave formation and wave turbulence in fibre optics.

The fact that nonlinear systems with several modes exhibit recurrence to the initial state after complex coupling dynamics, instead of equipartition, is known as the Fermi–Pasta–Ulam (FPU) paradox[1,2]. The controversial nature of such phenomena has stimulated several decades of prolific investigations. The final emerging picture is that the equipartition is eventually reached, though over extremely long times, whereas recurrences dominate the behaviour over shorter timescales[3]. In dispersive and nonlinear systems that represent the continuous limit of the oscillator chains originally considered by FPU, a similar behaviour is envisaged. In particular, in optical fibres where the propagation is ruled by the nonlinear Schrödinger equation (NLSE), FPU recurrence is triggered by the universal phenomenon of modulational instability, that is, the exponential growth of a modulation at the expense of a strong pump[4,5]. Modulational instability induces a seeded modulation frequency to be amplified along with its harmonics via multi-wave mixing to form a comb with a spectral triangular shape, until the process is reversed leading to FPU recurrence[6]. To date, in single-pass optical experiments, observations have been limited to the first recurrence cycle[7–9], whereas the long-term dynamics is conjectured to lead to a thermalized state owing to the role played by amplified noise[10].

The investigation of such phenomena are attracting tremendous interest in optics[11–26], boosted by their strong link with the formation of deterministic breathers[23], statistics of rogue waves[25,26], supercontinuum generation[24], turbulence[11,15] and frequency combs in microresonators[13]. Yet, in this context, the essential fact that nonlinear modulational instability does not involve a simple recurrence, but rather a complicated phase-space structure[27–32] associated with spontaneous symmetry breaking[33], has never been observed. The signature of such a structure is the occurrence of two types of qualitatively different recurrences that are accessible under the same operating conditions. Observation of this phenomenon, however, has been elusive so far due to fundamental limitations in the experiments. The major limitation is losses, which prevent the observation of both types of recurrence, as recently shown in water-wave experiments[34] (which are also affected by higher-order effects[35]). An additional limitation, in fibre optics, comes from the need to measure the longitudinal variation of the phases of the mixing products, which turns out to be extremely challenging. In this study, we overcome both these limitations in a fibre experiment by introducing (1) a loss compensation scheme and (2) a novel measurement technique that allows the powers and relevant phases along the fibre to be mapped. As a result, we clearly observe the signature of the spontaneously broken symmetry of FPU recurrence.

Phase-space structure of recurrent modulational instability

The modulational instability and its recurrent FPU stage are described by the NLSE that rules the propagation of the electric field envelope $E(Z,T)$ in the anomalous dispersion regime of an optical fibre:

$$i\frac{\partial E}{\partial Z}-\frac{\beta_2}{2}\frac{\partial^2 E}{\partial T^2}+\gamma|E|^2E=0 \quad (1)$$

where γ is the nonlinear coefficient, β_2 is the negative (anomalous) group-velocity dispersion, Z is the distance and T is the retarded time. According to equation (1), modulational instability involves the growth with exponential gain $g(\omega)$ (see Fig. 1a) of a modulation with frequency f_m (sideband pair with frequency detuning $\pm f_m$) at the expense of a continuous wave pump with power P, provided that the normalized frequency $\omega=2\pi f_m\sqrt{|\beta_2|/\gamma P}$ is such that $\omega\leq 2$. When such instability is seeded, FPU cycles of amplification and back-conversion occur[7–9,27–32]. To understand the richness and complexity of the recurrence, the key point is that the onset of modulational instability implies a spontaneous symmetry breaking, as sketched in Fig. 1a. Indeed the mixing process is equivalent to the motion of an ideal particle in the potential sketched in Fig. 1a, where the equilibrium point at the origin corresponds to

[1]University of Lille, CNRS, UMR 8523 - PhLAM - Physique des Lasers Atomes et Molécules, Lille, France. [2]Department of Engineering, University of Ferrara, Ferrara, Italy. *e-mail: arnaud.mussot@univ-lille1.fr; stefano.trillo@unife.it

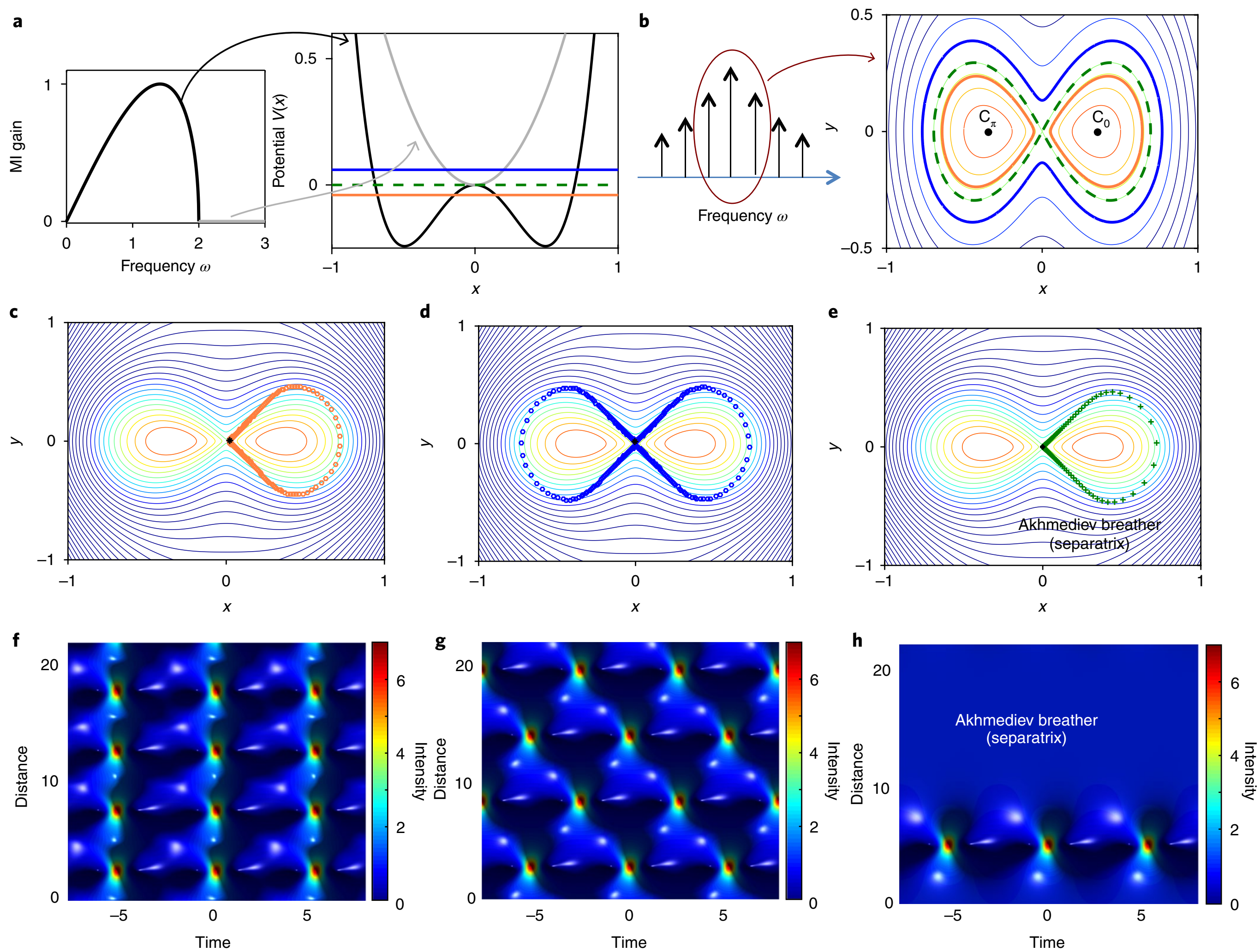

Fig. 1 | Spontaneous symmetry-breaking of modulational instability and FPU. a, Modulational instability (MI) gain versus ω and sketch of the equivalent potential associated with the mixing process, exhibiting spontaneous symmetry breaking (change from single to double well) when going across the onset of modulational instability at $\omega = 2$. **b**, Phase-plane evolutions in the plane $(x,y) \equiv (\eta_1\cos\Delta\phi, \eta_1\sin\Delta\phi)$, as obtained from the simple oscillator (Hamiltonian in equation (2), where $\omega = 1.25$ as in the experiment) describing the interaction of the pump and first-order sidebands, as can be seen from the schematic of the comb; the separatrix (dashed green line) and the inner and outer orbits (thick orange and blue solid lines, respectively) correspond to motions characterized by the total energy levels reported with the same colour in **a**. **c–e**, Projections of NLSE trajectories (open dots) on the 3WM phase plane (x,y) for weak initial modulation with different initial phases: $\Delta\phi_0 = 0$ (**c**), $\Delta\phi_0 = \pi/2$ (**d**) and $\Delta\phi_0 = -0.285\pi$ (**e**). **f–h**, Corresponding full temporal evolutions obtained from the NLSE showing in-phase (**f**) and out-of-phase (staggered; **g**) recurrences, and the separatrix or Akhmediev breather (**h**). The distance and time are in units nonlinear length $Z_{nl} = (\gamma P)^{-1}$ and characteristic time $T_0 = \sqrt{|\beta_2|Z_{nl}}$, respectively.

the pump wave. Decreasing ω across the onset of modulational instability induces the potential to undergo a spontaneous symmetry-breaking transition from a single well (with the minimum representing the stable pump for $\omega > 2$) to a double well for $\omega < 2$, where the pump exchanges its stability with two new minima. The simplest formalization of this concept, which allows the prominent role of the phases in the dynamics to be emphasized, is the truncation to three-wave mixing (3WM)[31,36], according to which the mixing can be described in terms of a one-dimensional oscillator by a Hamiltonian (see Methods; for a discussion of other approaches see also Supplementary Information):

$$H = \eta_1(1-\eta_1)\cos(2\Delta\phi) + (1-\omega^2/2)\eta_1 - 3\eta_1^2/4 \qquad (2)$$

where η_1 is the power fraction of the first-order ($n = 1$) sidebands and $\Delta\phi = \phi_0 - \phi_1$ is the only effective phase, ϕ_0 and ϕ_1 being the pump and sideband phase, respectively. The level curves of H, shown in Fig. 1b in the plane $(x,y) \equiv (\eta_1\cos\Delta\phi, \eta_1\sin\Delta\phi)$, clearly show the double-loop structure characteristic of the motion in a double-well potential in x. The centres or stable points C_0 and C_π correspond to the minima of the potential and are the 3WM representation of invariant modulated waves with equal modulation depth and opposite sideband phase $\Delta\phi = 0$ or $\Delta\phi = \pi$ (relative to the pump). In the time domain, they stand for identical wavetrains except for a temporal shift of half period π/ω due to such shift. A separatrix or homoclinic loop (dashed green curve in Fig. 1b) divides the possible trajectories into: (1) inner orbits (thick orange curve in Fig. 1b, corresponding to evolutions in a single well) surrounding only one stable centre, either C_0 or C_π, thus experiencing phase variations bounded in one (right or left) semiplane; and (2) outer orbits or double-well evolutions (thick blue curve in Fig. 1b), surrounding both stable centres and hence featuring unconstrained phase variations in the whole range $[0,2\pi]$. In particular, in this case, maximum depletion is obtained by alternation between $\Delta\phi = 0$ and $\Delta\phi = \pi$, corresponding to temporal wavetrains mutually shifted by half period.

We are interested in the so-called homoclinic crossing phenomenon[27–32], that is, switching between type (1) and type (2) orbits controlled by the launching conditions. For a weakly modulated pump, this occurs in the whole range of unstable frequencies, by changing the input phase $\Delta\phi_0 = \Delta\phi\ (z=0)$ from amplitude modulation $\Delta\phi_0 = 0$ to frequency modulation $\Delta\phi_0 = \pi/2$ (other conditions for switching become frequency dependent and are discussed in the Supplementary Information). We show this by means of direct numerical integration of the NLSE. Figure 1c–e shows the projections of the NLSE evolutions on the 3WM phase plane for $\Delta\phi_0 = 0$, $\Delta\phi_0 = \pi/2$ and $\Delta\phi_0 = -0.285\pi$ (separatrix), respectively. Apart from slight quantitative deviations (due to the neglected higher-order sidebands), the orbits present exactly the same qualitative features expected from 3WM. The corresponding spatio-temporal evolutions presented in Fig. 1f–h show that homoclinic crossing implies, as expected, switching from the unshifted recurrences shown in Fig. 1f to the staggered patterns shown in Fig. 1g induced by the shift $\Delta\phi = \pi$, periodically acquired only by the double-loop orbits. Finally, the separatrix in Fig. 1h represents the well-known exact solution of the NLSE known as the Akhmediev breather[23,24,26,27,31].

To further show that the qualitatively different FPU recurrences associated with the homoclinic crossing can be detected in an optical fibre, in Fig. 2, we show further simulations based on the full NLSE with realistic real-world values. We find that, for a very weak input modulation (pump to sideband power ratio of 20 dB, or $\eta_1 = 0.98$), nearly 18 km of optical fibre are necessary to see two recurrences with $\Delta\phi_0 = 0$, as shown in Fig. 2a–d, whereas with $\Delta\phi_0 = \pi/2$ only one full recurrence is completed over the same length. Indeed, while in both cases two cycles of conversion and back-conversion are achieved in terms of powers (see full spectra in Fig. 2c,g or power fractions in Fig. 2a,e), when $\Delta\phi_0 = \pi/2$, the phase, which spans the whole range $[0,2\pi]$, recurs only over a double distance. Indeed, in the latter case, the initial condition in the phase plane is recovered only after moving through the double loop shown in Fig. 2h, which requires nearly twice the distance needed to move through a single loop as in Fig. 2d. Interestingly, in both cases, the weakness of the input modulation induces the conversion process, which is very rapid around the maximum extension of the comb, to strongly slow down near the recurrences (see the plateau in power in Fig. 2a,e) when the point passes, in the phase plane, close to the saddle point (that is, the unstable pump). This is similar to the behaviour of a pendulum[37] or any other nonlinear oscillator with an unstable state.

Experimental characterization of the evolutions

To have an almost real-time access to the ongoing dynamics along the fibre, we have developed a multi-channel vector optical-time-domain reflectometer. It is optimized for nonlinear measurements. Indeed, Rayleigh backscattered light excited from a coherent light source exhibits a jagged appearance due to the fading phenomenon. The latter originates from the random state of polarization of the scattered light and from a speckle-like phenomenon due to the huge number of scattered waves involved in the process[38]. To overcome this strong limitation, we perform an error correction calibration using a double pulse sequence. A strong signal pulse is first launched

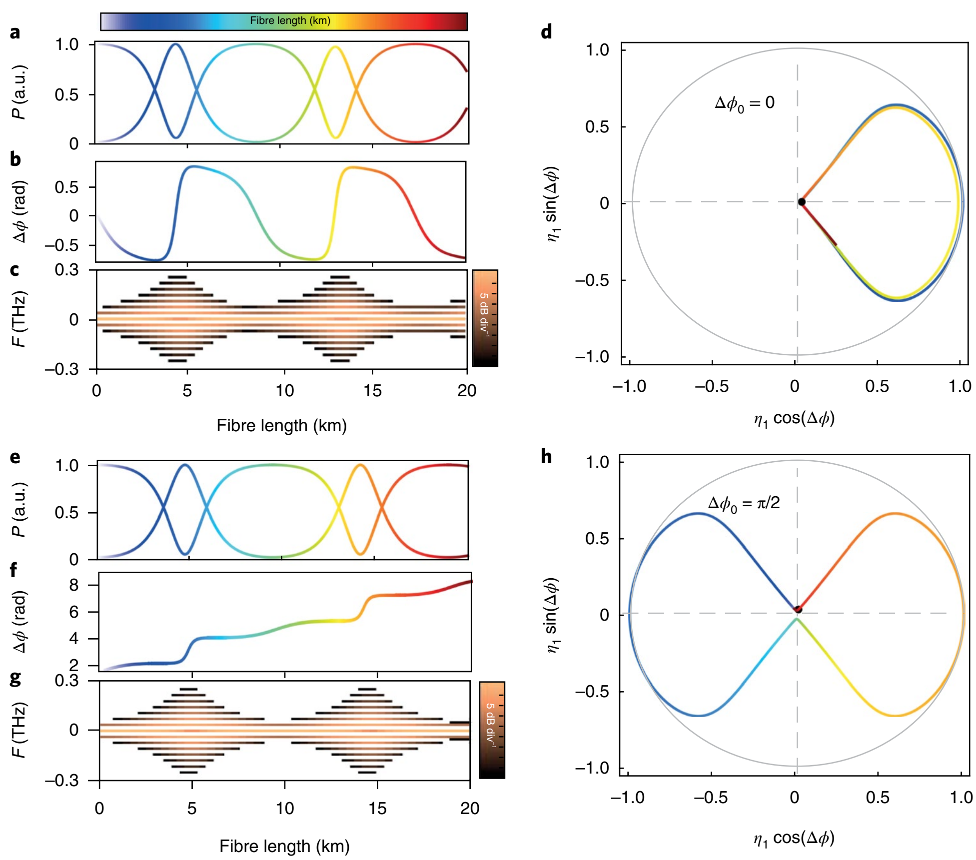

Fig. 2 | Homoclinic crossing and period doubling in fibre FPU recurrence. a–c,e–g, Evolutions along fibre distance of pump and sideband powers (**a**,**e**), effective phase $\Delta\phi(Z)$ (**b**,**f**) and full modulational instability power spectrum (**c**,**g**). **d**,**h**, Phase-plane portrait of the evolution. Upper panels (**a–d**) and lower panels (**e–h**) differ only in the input relative phase, set to $\Delta\phi_0 = 0$ (amplitude modulation) and $\Delta\phi_0 = \pi/2$ (frequency modulation), respectively. Fibre parameters: $\beta_2 = -19\ \mathrm{ps^2\,km^{-1}}$, $\gamma = 1.3\ (\mathrm{W\,km})^{-1}$, modulation frequency $f_m = 35$ GHz, pump power $P = 450$ mW, pump to signal input power ratio is equal to 20 dB. All power plots are normalized to their respective maxima.

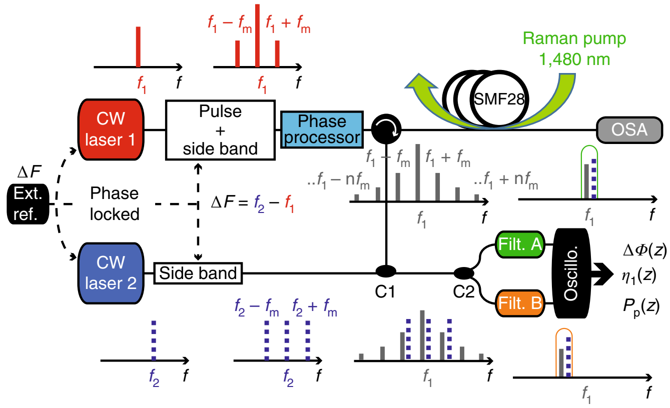

Fig. 3 | The novel measurement technique. Basic diagram of the experimental setup. $f_{1,2}$ are the frequencies of the main laser and the local oscillator laser, respectively, with $\Delta F = f_1 - f_2 = 800$ MHz. Here $f_m = 35$ GHz is the input modulation frequency (that is, pump frequency at f_1, input sideband frequencies at $f_1 \pm f_m$). Modulational instability evolution is studied in the 7.7-km-long single-mode fibre (SMF28). The backscattered signal from the SMF28 goes through a circulator and is analysed via heterodyning (beating with the local oscillator) and then filtered (filters A and B) to isolate the power and phase evolutions of the pump and the first-order sideband pair in the modulational instability spectral comb.

inside the experiment fibre (SMF28) and a weak reference pulse, typically attenuated by 13 dB, shortly follows. We assume that the weak pulse and its backscattered light experiences similar linear effects compared to the strong one, but negligible nonlinear effects. We then correct the amplitude and phase of each strong backscattered wave by means of those of the weak one. Figure 3 shows a simplified overview of the experimental setup (see Supplementary Information for a more thorough discussion and description). After the pulse modulation stage, the incoming light is phase modulated at $f_m = 35$ GHz to generate two phase-locked symmetric sidebands that initiate the FPU process. Owing to a commercial waveshaper, we have full arbitrary control of the relative phase and intensity of these sidebands with respect to the carrier, that is, the pump. In addition, along the fibre, a counter-propagating Raman pump (1,480 nm) accurately compensates for the linear losses of the SMF28. On the detection side, the Rayleigh backscattered light is mixed with a local oscillator. To perform a coherent heterodyne detection, the local oscillator is phased locked and detuned by $\Delta F = 800$ MHz with respect to the pump frequency. To provide a local oscillator to each optical component of interest, the local oscillator is also modulated at $f_m = 35$ GHz. The analysis is restricted to the evolution of the pump and the signal (first-order sideband pair) as they contain all the information needed to characterize the whole dynamics of our system (see Methods). The time of flight of their beat note with the modulated local oscillator is isolated with an optical filter, and logged with a real-time oscilloscope for further demodulation processing. Finally, a spatial resolution of about 20 m is achieved.

Discussion

In the experiment, the modulation frequency is set to $f_m = 35$ GHz, that is, slightly below the peak modulational instability gain (nonlinear phase matching) frequency at 40 GHz, and such that all the harmonics nf_m $n = 2, 3, \ldots$ are stable, thereby experiencing synchronous growth and decay with the main injected pair[20]. The input spectrum in the SMF28 (see Fig. 4a) clearly shows the three main input frequencies, along with very weak (<−25 dB) harmonics due to residual four-wave mixing in the fibres used to carry the signal to the main SMF28 fibre. Figure 4b shows the output triangular spectrum under maximal temporal compression. Using our setup, we have recorded experimentally the longitudinal evolutions of the powers of the pump and of the first-order sideband and their relative phase for two different initial pump-signal relative phase values ($\Delta\phi_0 = 0$ and $\Delta\phi_0 = \pi/2$). All the evolutions are shown in Fig. 4c–h with solid rainbow lines. Ideally, one should use a very weak modulation at the input. However, this results in a large conversion and large recurrence distances, which in turn makes the compensation scheme more demanding due to the increased losses and enhances the impact of noise amplification due to spontaneous modulational instability, which is ultimately responsible for thermalization[10]. In our experiment, the trade-off between a weak modulation and reasonable fibre length led us to operate with a pump to sideband power ratio of 8.5 dB (compared with 20 dB in the ideal case of Fig. 2), which allowed for scaling down two recurrence periods below the length of 7.7 km of our fibre. It is noteworthy that such a stronger modulation results in a less pronounced plateau in power (see Fig. 4c,f, and compare with Fig. 4a,e), due to passages at larger distances from the saddle point (that is, the pump) in the phase plane. Interestingly enough, by comparing Fig. 4c and Fig. 4d, we notice a nearly perfect recurrence in terms of power levels for $\Delta\phi_0 = \pi/2$, whereas the recurrence is within 20% for $\Delta\phi_0 = 0$, desspite the same level of Raman pump to compensate for the losses. We mainly attribute this to the fact that, in the presence of strong two sidebands modulation, the trajectories followed by the injected amplitude modulation ($\Delta\phi_0 = 0$) show a stronger deviation against the ideal case of weak modulation (Fig. 4), compared with the case of the injected frequency modulation ($\Delta\phi_0 = \pi/2$). This is indeed evident also from the simulated trajectories (black curves) in Fig. 4c,f, which highlight the non-ideal behaviour that is also manifest from a slight spatial shift between the dip of the pump and the peak of the sidebands as well as a certain degree of asymmetry between the first cycle and the second, which also reflects in the non-perfect superposition of the trajectories in the phase plane (compare Figs. 2d and 4e).

Nonetheless, we emphasize that the measured data clearly highlight the two qualitatively different types of recurrences. Indeed the range of variation of the phase is bounded between ±1 rad for $\Delta\phi_0 = 0$ (see Fig. 4d), whereas for $\Delta\phi_0 = \pi/2$ the phase turns out to span nearly the whole range of 2π over a single recurrence (see Fig. 4g). The evidence for the impact of the relative initial phase is even more clear by reconstructing the phase-portrait evolutions. For $\Delta\phi_0 = 0$, as shown in Fig. 4e, the evolution exhibits more than two quasi-periodic orbits spanning only half of the phase plane, as predicted in the ideal scenario (Fig. 2a–d). Conversely, for $\Delta\phi_0 = \pi/2$, the phase-plane evolution in Fig. 4h spans the whole phase plane making two loops that are nearly symmetric around the vertical axis. All the results are confirmed by numerical simulations of the NLSE (equation (1)), with good agreement (solid black lines). We have also performed additional measurements corresponding to initial conditions located on the other cardinal points of the phase plane, that is, $\Delta\phi_0 = \pi$, $3\pi/2$, which show good agreement with the expected dynamics. Indeed, we found that symmetric initial conditions in the phase plane, $\Delta\phi_0 = \pm\pi/2$ and $\Delta\phi_0 = 0$, π, respectively, give almost symmetric orbits in the phase plane (see Supplementary Information). Importantly, we have also provided further evidence for homoclinic crossing by performing additional measurements obtained by varying the phase across the critical value fixed by the slope of the separatrix near the origin (see Supplementary Information). These measurements become increasingly difficult because the period of the recurrence tends to diverge when such a critical value is approached.

Conclusions

We believe that our experimental technique opens new perspectives in the characterization of parametric mixing processes in guided wave optics, including the regime of phase-sensitive amplification. Our results pave the way towards a more complete understanding

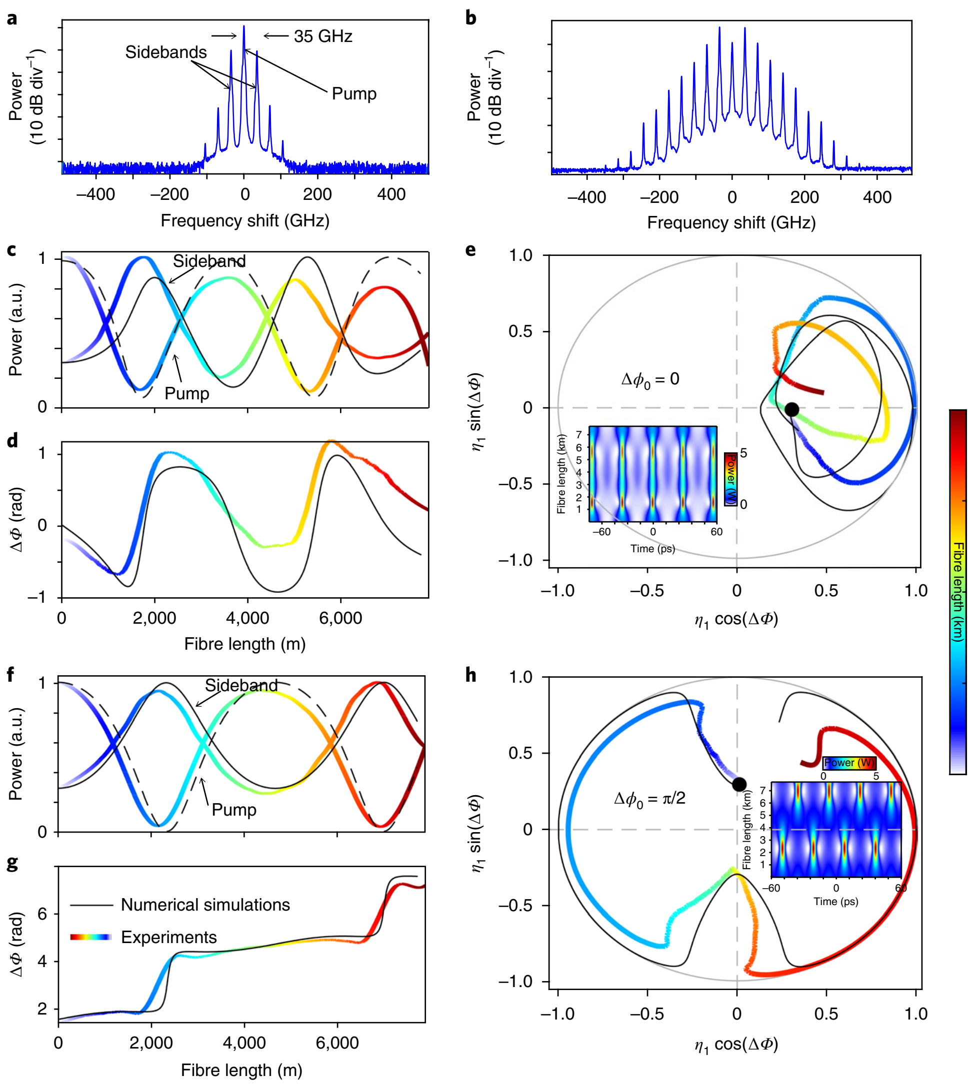

Fig. 4 | Observed recurrences and their phase-plane projections. a,b, Spectra at the input of the SMF28 (**a**) and the fibre output recorded with an optical spectrum analyser by slightly decreasing the sideband amplitude to shift the maximal compression point at the fibre output (**b**). **c**,**d**,**f**,**g**, Evolution along the fibre length of the pump power (dashed lines) and the first sideband pair power (dotted lines; **c**,**f**) and the relative phase $\Delta\phi(z)$ (**d**,**g**). **e**,**h**, Projections of the evolutions in the 3WM phase plane (the insets show the corresponding evolutions obtained numerically from the NLSE). Numerical simulations are depicted in black lines and experiments in solid rainbow lines. **c**–**e** and **f**–**h** differ only in the initial relative phase of the modulation, $\Delta\phi_0=0$ and $\Delta\phi_0=\pi/2$, respectively. Parameters as in Fig. 2 except for the fibre length, which is 7.7 km, and the pump to signal input power ratio, which is 8.5 dB. All power plots are normalized to their respective maxima.

of the extremely rich and formidably complex phenomenon of FPU recurrence. In this respect, it must be noted that most of the recent progress towards understanding the recurrence and its deterioration have a theoretical nature (see, for example, refs [3,10,11] and references therein). However, few experimental tests exist that deepen the mechanisms of mode interaction and the recurrence in a truly conservative (Hamiltonian) setting, as originally proposed by FPU. Our results establish optical fibres to be a viable platform for investigating all aspects of mode interactions, including the role of the mutual phases, at the same time highlighting for the role of spontaneous symmetry breaking and the existence of a complex homoclinic structure in FPU dynamics ruled by modulational instability. This opens the doors to further experimental investigations that range from the mechanisms of thermalization and their universality[10,11], the observation of higher-order separatrices, their associated phase-plane dynamics and their role in rogue-wave formation[25] and supercontinuum generation, the link with new mechanisms of soliton-mediated recurrences in fibres[39], to the transition to chaos induced around the homoclinic structure (homoclinic chaos) in strongly perturbed structures such as fibre passive cavities and microresonators for frequency comb generation[13], where modulational instability remains a key driving mechanism.

Methods

Methods, including statements of data availability and any associated accession codes and references, are available at https://doi.org/10.1038/s41566-018-0136-1.

Received: 12 July 2017; Accepted: 21 February 2018;
Published online: 02 April 2018

References

1. Fermi, E., Pasta, J. & Ulam, S. in *Collected Papers of Enrico Fermi* Vol. 2 (ed. Segré, E.) 977–988 (Univ. Chicago Press, Chicago, Illinois, 1965).
2. Porter, M. A., Zabusky, N. J., Hu, B. & Campbell, D. K. Fermi, Pasta, Ulam and the birth of experimental mathematics. *Am. Sci.* **97**, 214–221 (2009).

3. Onorato, M., Vozella, L., Proment, D. & Lvov, Y. V. Route to thermalization in the α-Fermi–Pasta–Ulam system. *Proc. Natl Acad. Sci. USA* **112**, 4208–4213 (2015).
4. Tai, K., Hasegawa, A. & Tomita, A. Observation of modulation instability in optical fibers. *Phys. Rev. Lett.* **56**, 135–138 (1986).
5. Zakharov, V. E. & Ostrovsky, L. A. Modulation instability: the beginning. *Phys. D* **238**, 540–548 (2009).
6. Akhmediev, N. N. Nonlinear physics: déjà vu in optics. *Nature* **413**, 267–268 (2001).
7. Van Simaeys, G., Emplit, Ph. & Haelterman, M. Experimental demonstration of the Fermi–Pasta–Ulam recurrence in a modulationally unstable optical wave. *Phys. Rev. Lett.* **87**, 033902 (2001).
8. Van Simaeys, G., Emplit, Ph. & Haelterman, M. Experimental study of the reversible behaviour of modulational instability in optical fibres. *J. Opt. Soc. Am. B* **19**, 477–486 (2002).
9. Beeckman, J., Hutsebaut, X., Haelterman, M. & Neyts, K. Induced modulation instability and recurrence in nematic liquid crystals. *Opt. Express* **18**, 11185–11195 (2007).
10. Wabnitz, S. & Wetzel, B. Instability and noise-induced thermalization of Fermi–Pasta–Ulam recurrence in the nonlinear Schrödinger equation. *Phys. Lett. A* **378**, 2750–2756 (2014).
11. Guasoni, M. et al. Incoherent Fermi–Pasta–Ulam recurrences and unconstrained thermalization mediated by strong phase correlations. *Phys. Rev. X* **7**, 011025 (2017).
12. Grinevich, P. G. & Santini, P. M. The exact rogue wave recurrence in the NLS periodic setting via matched asymptotic expansions, for 1 and 2 unstable modes. Preprint at https://arxiv.org/abs/1708.04535 (2017).
13. Bao, C. et al. Observation of Fermi–Pasta–Ulam recurrence induced by breather solitons in an optical microresonator. *Phys. Rev. Lett.* **117**, 163901 (2016).
14. Närhi, M. et al. Real-time measurements of spontaneous breathers and rogue wave events in optical fibre modulation instability. *Nat. Commun.* **7**, 13675 (2016).
15. Soto-Crespo, J. M., Devine, N. & Akhmediev, N. Integrable turbulence and rogue waves: breathers or solitons? *Phys. Rev. Lett.* **116**, 103901 (2016).
16. Kibler, B., Chabchoub, A., Gelash, A. N., Akhmediev, N. & Zakharov, V. E. Super-regular breathers in optics and hydrodynamics: omnipresent modulation instability beyond simple periodicity. *Phys. Rev. X* **5**, 041026 (2015).
17. Toenger, S. et al. Emergent rogue wave structures and statistics in spontaneous modulation instability. *Sci. Rep.* **5**, 10380 (2015).
18. Bendhamane, A. et al. Optimal frequency conversion in the nonlinear stage of modulation instability. *Opt. Express* **23**, 30861–30871 (2015).
19. Biondini, G. & Mantzavinos, D. Universal nature of the nonlinear stage of modulational instability. *Phys. Rev. Lett.* **116**, 043902 (2016).
20. Chin, S. A., Ashour, O. A. & Belić, M. R. Anatomy of the Akhmediev breather: cascading instability, first formation time, and Fermi–Pasta–Ulam recurrence. *Phys. Rev. E* **92**, 063202 (2015).
21. Mussot, A., Kudlinski, A., Droques, M., Szriftgiser, P. & Akhmediev, N. Fermi–Pasta–Ulam recurrence in nonlinear fiber optics: the role of reversible and irreversible losses. *Phys. Rev. X* **4**, 011054 (2014).
22. Erkintalo, M. et al. Higher-order modulation instability in nonlinear fibre optics. *Phys. Rev. Lett.* **107**, 253901 (2011).
23. Kibler, B. et al. The Peregrine soliton in nonlinear fibre optics. *Nat. Phys.* **6**, 790–795 (2010).
24. Dudley, J. M., Genty, G., Dias, F., Kibler, B. & Akhmediev, N. Modulation instability, Akhmediev breathers and continuous wave supercontinuum generation. *Opt. Express* **17**, 21497–21508 (2009).
25. Onorato, M., Residori, S., Bortolozzo, U., Montina, A. & Arecchi, F. T. Rogue waves and their generating mechanisms in different physical contexts. *Phys. Rep.* **528**, 47–89 (2013).
26. Dudley, J. M., Dias, F., Erkintalo, M. & Genty, G. Instabilities, breathers and rogue waves in optics. *Nat. Photon.* **8**, 755–764 (2014).
27. Akhmediev, N. N., Eleonoskii, V. M. & Kulagin, N. E. Generation of periodic trains of picosecond pulses in an optical fibre: exact solutions. *Sov. Phys. JETP* **62**, 894–899 (1985).
28. Akhmediev, N. N., Eleonskii, V. M. & Kulagin, N. E. Exact first-order solutions of the nonlinear Schrödinger equation. *Theor. Math. Phys.* **72**, 809–818 (1987).
29. Ablowitz, M. J. & Herbst, B. M. On homoclinic structure and numerically induced chaos for the nonlinear Schrödinger equation. *SIAM J. Appl. Math.* **50**, 339–351 (1990).
30. Moon, H. T. Homoclinic crossings and pattern selection. *Phys. Rev. Lett.* **64**, 412–414 (1990).
31. Trillo, S. & Wabnitz, S. Dynamics of the modulational instability in optical fibers. *Opt. Lett.* **16**, 986–988 (1991).
32. Trillo, S. & Wabnitz, S. Self-injected spatial mode locking and coherent all-optical FM/AM switching based on modulational instability. *Opt. Lett.* **16**, 1566–1568 (1991).
33. Liu, C. Spontaneous symmetry breaking and chance in a classical world. *Philos. Sci.* **70**, 590–608 (2003).
34. Kimmoun, O. et al. Modulation Instability and phase-shifted Fermi–Pasta–Ulam recurrence. *Sci. Rep.* **6**, 28516 (2016).
35. Ablowitz, M. J., Hammack, J., Henderson, D. & Schober, C. M. Modulated periodic Stokes waves in deep water. *Phys. Rev. Lett.* **84**, 887–890 (2000).
36. Cappellini, G. & Trillo, S. Third-order three-wave mixing in single-mode fibres: exact solutions and spatial instability effects. *J. Opt. Soc. Am. B* **8**, 824–834 (1991).
37. Butikov, E. I. The rigid pendulum—an antique but evergreen physical model. *Eur. J. Phys.* **20**, 429–441 (1999).
38. Healey, P. Fading in heterodyne OTDR. *Electron. Lett.* **20**, 30–32 (1984).
39. Deng, G., Li, S., Biondini, G. & Trillo, S. Recurrence due to periodic multisoliton fission in the defocusing nonlinear Schrödinger equation. *Phys. Rev. E* **96**, 052213 (2017).

Acknowledgements

This work was partly supported by the Agence Nationale de la Recherche through the High Energy All Fiber Systems (HEAFISY) and Nonlinear dynamics of Abnormal Wave Events (NoAWE) projects, the Labex Centre Europeen pour les Mathematiques, la Physique et leurs Interactions (CEMPI) and Equipex Fibres optiques pour les hauts flux (FLUX) through the 'Programme Investissements d'Avenir', by the Ministry of Higher Education and Research, Hauts de France council and European Regional Development Fund (ERDF) through the Contrat de Projets Etat-Region (CPER Photonics for Society, P4S) and FEDER through the HEAFISY project.

Author contributions

A.M. and P.S. conceived the experimental setup. A.M., C.N., A.K., F.C. and P.S. worked on the experiment. M.C. and S.T. developed the theoretical aspects. A.M., S.T., M.C. and C.N. performed numerical simulations. All authors contributed to analysing the data and writing the paper.

Competing interests

The authors declare no competing interests.

Additional information

Supplementary information is available for this paper at https://doi.org/10.1038/s41566-018-0136-1.

Reprints and permissions information is available at www.nature.com/reprints.

Correspondence and requests for materials should be addressed to A.M. or S.T.

Publisher's note: Springer Nature remains neutral with regard to jurisdictional claims in published maps and institutional affiliations.

Methods

Numerics. The simulations reported in Figs. 1 and 2 are made by integrating the NLSE (equation (1)) with a pseudospectral or split-step method with typical grid spacing $\Delta T = 0.5$ ps and $\Delta Z = 5$ cm. Boundary conditions are implicitly imposed on temporal windows that are a multiple of the modulation period $T_m = 1/f_m$. The initial condition is set to $E(Z,T) = \sqrt{P_p} + \sqrt{P_s}\exp(-i\Delta\phi_0)\,[\exp(i2\pi f_m T) + \exp(-i2\pi f_m T)]$, where P_p and P_s are the pump and sideband power, respectively, which fix the pump to signal power ratio $10\log_{10}P_p/P_s$ given in the text (20 dB in Fig. 2 or 8.5 dB in Fig. 4, corresponding to $P_s = 4.5$ mW and $P_s = 63.6$ mW, respectively). We have also checked numerically that higher-order dispersion terms, as well as the Raman effect have a negligible impact on our results and can be neglected, so that the whole dynamics of the system can be accurately captured by the NLSE.

Theory. Starting from the NLSE, the description of the nonlinear stage of modulational instability in terms of the reduced oscillator (2), can be obtained as follows. The comb that develops from depleted modulational instability is of the form $E(Z,T) = \sqrt{P}\sum_n a_n(Z)\exp(i2\pi f_m T)$, where the sum is over all integers $n = \ldots, -2, -1, 0, 1, 2, \ldots$, f_m is the input modulation frequency and P is the injected (conserved) power, $a_0(Z)$ and $a_{\pm|n|}(Z)$ are the complex amplitudes of the pump and the nth sideband pair, respectively. As the spectrum is triangular[24] with strong decay between adjacent sidebands of increasing order ($|a_{n+1}|^2/|a_n|^2(\mathrm{dB}) = 10\log_{10}(2-\omega)/(2+\omega)$ at conversion apex, for example, ~−8 dB at peak gain $\omega = \sqrt{2}$, as shown in ref. [18]), we can accurately approximate the process by means of three modes (3WM, $n = -1, 0, 1$), neglecting higher-order sidebands $|n| \geq 2$ that remain enslaved and phase-locked to the main pair $n = \pm 1$ on propagation. Hence, further assuming symmetric sidebands ($a_1 = a_{-1}$) as in the experiment, we plug into the NLSE (equation (1)) the 3WM ansatz $E(Z,T) = \sqrt{P}\{a_0(Z) + a_1(Z)[\exp(i2\pi f_m T) + \exp(-i2\pi f_m T)]/\sqrt{2}\}$, and obtain coupled equations by grouping terms at the same frequency. Then, following the approach developed in refs. [31,36], we exploit the Hamiltonian structure of the resulting system of equations to reduce them to a one degree of freedom oscillator in terms of the conjugated variables $\eta_1 = |a_1|^2 = 1 - |a_0|^2$ and $\Delta\phi = \phi_0 - \phi_1$, which are found to obey the following evolution equations:

$$\begin{aligned}\frac{d\eta_1}{dz} &= \frac{\partial H}{\partial \Delta\phi} = -2\eta_1(1-\eta_1)\sin(2\Delta\phi)\\ \frac{d\Delta\phi}{dz} &= -\frac{\partial H}{\partial \eta_1} = \left(\frac{\omega^2}{2} - 1\right) + \frac{3}{2}\eta_1 + (2\eta_1 - 1)\cos(2\Delta\phi)\end{aligned} \qquad (3)$$

where $z = Z/Z_{nl}$ is the normalized distance in units of the nonlinear length $Z_{nl} = (\gamma P)^{-1}$. Clearly, $H = H(\eta_1, \Delta\phi)$ in equation (3) takes the expression of the Hamiltonian reported in equation (2). The invariance of H along the motion allows the level curves reported in Fig. 1b to be drawn.

Experiment. Two major challenges faced in the experiment are: (1) the loss compensation in the 7.7-km-long SMF28, that would induce all the evolutions to drop on phase-shifted evolution[34], thus hiding the broken symmetry of FPU; (2) to overcome the fading phenomenon that is likely to occur when a quasi-monochromatic wave is launched in an optical fibre[38]. The losses of the SMF28 are almost perfectly compensated by means of a scheme borrowed by telecommunication systems, which exploits a counter-propaganting wave centred at 1,480 nm acting as a Raman pump (see Fig. 3 and Supplementary Information for further information). Concerning the second issue, we remind that a random noise in amplitude and phase is superimposed on the backscattered light originating from variations of the state of the polarization of the light and/or from local thermomechanical fluctuations of the scattering volume. We removed the contribution of this detrimental linear phenomenon on the reflected pulse as follows. We launched two consecutive pulses in the fibre. The first one is strong and is responsible for the nonlinear dynamics, whereas a following weaker one (−13 dB) experiences essentially linear effects. These linear effects are similar to those experienced by the first strong pulse because the time delay between these pulses is extremely short (only 102 μs) compared with the characteristic response time of thermomechanical fluctuations in the fibre. The amplitude and the phase of the backscattered strong signal is then corrected by means of the weak one. This scheme allows the contribution of the fading effect to be effectively removed (the effectiveness of the scheme is further discussed in the Supplementary Information, which shows a typical trace before and after the correction in Supplementary Fig. 3).

The drawback of this method is that all linear contributions are removed, including the phase due to the group-velocity dispersion acquired during the propagation. This contribution is linked to the linear phase mismatch term of the four-photon process underlying the occurrence of modulational instability, and can not be neglected. However, it can be easily restored by adding to the compensated phase evolution the characteristic phase term arising from group velocity dispersion, that is, $\frac{1}{2}\beta_2(2\pi f_m)^2 Z$.

Data availability. Most of the relevant data used in this paper are contained in the Supplementary Information while further data are available from the corresponding authors upon reasonable request.